Available online at www.sciencedirect.com
SCIENCE DIRECT®
International Journal of Heat and Fluid Flow 26 (2005) 792–800
International Journal of HEAT AND FLUID FLOW
www.elsevier.com/locate/ijhff

Vertical gradient freezing using submerged heater growth with rotation and with weak magnetic and electric fields

A.M. Holmes [a], X. Wang [a], N. Ma [a,*], D.F. Bliss [b], G.W. Iseler [b]

[a] Department of Mechanical and Aerospace Engineering, North Carolina State University, Campus Box 7910, Rayleigh, NC 27695, USA
[b] US Air Force Research Laboratory, Sensors Directorate AFRL/SNHC, 80 Scott Road, Hanscom AFB, MA 01731, USA

Received 4 November 2004; accepted 2 February 2005
Available online 18 April 2005

Abstract

Investigations for the melt growth gallium-antimonide (GaSb) semiconductor crystals are underway at the US Air Force Research Laboratory at Hanscom Air Force Base by the vertical gradient freeze (VGF) method utilizing a submerged heater. Electromagnetic stirring can be induced in the gallium-antimonide melt just above the crystal growth interface by applying a weak radial electric current in the melt together with a weak axial magnetic field. A force convection in the melt can be induced by rotating the heater. This paper uses a Chebyshev spectral collocation method and investigates the effects of heater rotation and electromagnetic stirring on the melt motion during the VGF process using a submerged heater. Clockwise and counterclockwise rotations of the heater augment and opposes the flow induced by the electromagnetic stirring, respectively. The radial velocity along the crystal–melt interface is proportional to both the strength of the electromagnetic stirring and the clockwise rotation of the heater. A relatively low rotation rate in the clockwise direction significantly increases this radial velocity.

1. Introduction

Bulk gallium-antimonide (GaSb) semiconductor crystals with high optical transmission are extremely important for space-based imaging applications. These crystals can be grown from the liquid phase (melt) and the melt is typically doped with an element in order to give the crystal certain optical properties. The growth of these crystals from the melt is critically important because viable substrates which are compositionally uniform both within a wafer and from wafer to wafer are needed.

Bulk gallium-antimonide crystals can be grown from the melt by the liquid-encapsulated Czochralski (LEC) process or by the vertical gradient freeze (VGF) process. The LEC process is a top-seeded growth method that has distinct advantages because the crystal is viewed directly during growth and because there is no container in contact with the crystal. However, short-range compositional uniformity can be problematic due to buoyancy-driven convection in the melt, which randomly changes the composition of the melt in the boundary layer at the growth interface (Kuniholm and Ma, 2003). In addition, long-range crystal composition generally changes due to a changing melt composition for dopants with segregation coefficients not equal to unity (Morton et al., 2002). Relatively good long-range compositional uniformity was achieved for a non-stoichiometric Sb-rich melt by the LEC process by Ohmori et al. (1982). However, only 25% of the melt volume was solidified because the continual increase of antimony in the melt as crystal growth progressed eventually caused the crystal–melt interface to breakdown due to constitutional supercooling. In the early-90s, Ostrogorsky (1990) introduced a modification of the bottom-seeded VGF process in which a submerged heater separates the melt into two zones, namely, a lower melt

* Corresponding author. Tel.: +1 919 515 5231; fax: +1 919 515 7968.
E-mail address: nancy_ma@ncsu.edu (N. Ma).

0142-727X/$ - see front matter © 2005 Elsevier Inc. All rights reserved.
doi:10.1016/j.ijheatfluidflow.2005.02.001

and an upper melt. As crystal growth progresses, the crystal solidifies and the submerged heater is slowly raised in order to maintain a constant lower melt depth. Meyer and Ostrogorsky (1997) performed experimental studies of the flow visualization with rotation during the Bridgman process with a submerged heater. The lower melt is continuously replenished with liquid from the upper melt with a composition chosen to offset the increasing dopant level in the lower melt due to rejection at the crystal growth front for dopants with segregation coefficients less than unity. Unfortunately, there can be severe long-range axial segregation in the crystal if the process does not have a way to replenish the melt with a composition that offsets rejection of species along the crystal–melt interface (Farrell and Ma, 2004). Ostrogorsky and Müller (1994) have shown that this modified bottom-seeded VGF method produces crystals which exhibit much lower defect densities and much more dopant uniformity than crystals grown by the LEC process.

Since molten gallium-antimonide is a good electrical conductor, a radial electric current in the melt can be used together with an axial magnetic field to stir the melt in order to control the dopant distribution in the semiconductor crystal, which depends on the convective and diffusive transport of the dopant in the melt. Wang et al. (2005) have demonstrated that a radial electric current of a few amps in the presence of a weak axial magnetic field can produce significant stirring rates in a gallium-antimonide melt having a 50 mm diameter and 1 cm depth. Some of the advantages of electromagnetic (EM) stirring for bottom-seeded crystal growth are enhancement of the radial dopant uniformity, reduction of thermal stresses, minimizing of defect densities, and the ability to grow at faster rates.

The large number of adjustable crystal growth parameters and the larger number of ways to combine them makes process optimization through trial-and-error extremely tedious. Therefore, models that predict melt motion and heat transfer would be very useful for tailoring the melt motion in order to optimize the complex growth process in a timely fashion. In the present paper, we present a numerical model that treats the melt motion during the vertical gradient freeze (VGF) process using a rotating submerged heater and with a uniform, steady axial magnetic field and a steady radial electric current.

2. Melt motion

This paper treats the melt motion of selenium in a gallium-antimonide melt during the vertical gradient freeze crystal growth using a rotating submerged heater with an externally applied, uniform, steady, axial magnetic field $B\hat{\mathbf{z}}$ combined with a radial electric current. Here, B is the magnetic flux density, while $\hat{\mathbf{r}}$, $\hat{\theta}$ and $\hat{\mathbf{z}}$ are the unit vectors for the cylindrical coordinate system. Our dimensionless problem is sketched in Fig. 1. The coordinates and lengths are normalized by the outer electrode's inner radius R, which is equal to the crystal radius, so that γ_e is the dimensionless radius of the center electrode, γ_h is the dimensionless radius of the submerged fused-silica heater housing, and b is the dimensionless depth of the lower melt. The electrodes are made of AXF-5Q graphite, which is manufactured by Poco Graphite. This graphite has an electrical conductivity equal to 1.47×10^{11} S/m (Wang et al., 2005). A single crystal seed, which initiates solidification, lies at the bottom of the fused silica crucible. A graphite disc and a boron nitride disc lie below the crucible. These discs are cooled by a water-cooled hearth which removes heat along the bottom of the crucible. The power to the submerged heater above the lower melt and to the heaters adjacent to the periphery of the crucible are adjusted so that the crystal–melt interface is nearly planar, and the melt adjacent to the submerged heater is held at a uniform and constant temperature T_h. As the crystal at $z = \alpha t$ solidifies, the crystal–melt interface moves axially upward at the dimensionless rate $\alpha = U_g/U_c$, where U_g is the constant growth rate and U_c is the characteristic velocity of the melt while z is normalized by the crystal's radius R and t is time normalized by R/U_c. The lower melt is replenished with liquid supplied from an upper melt to a small annular gap between the submerged heater and the outer electrode. The submerged heater at $z = \alpha t + b$ moves upward at the same rate so

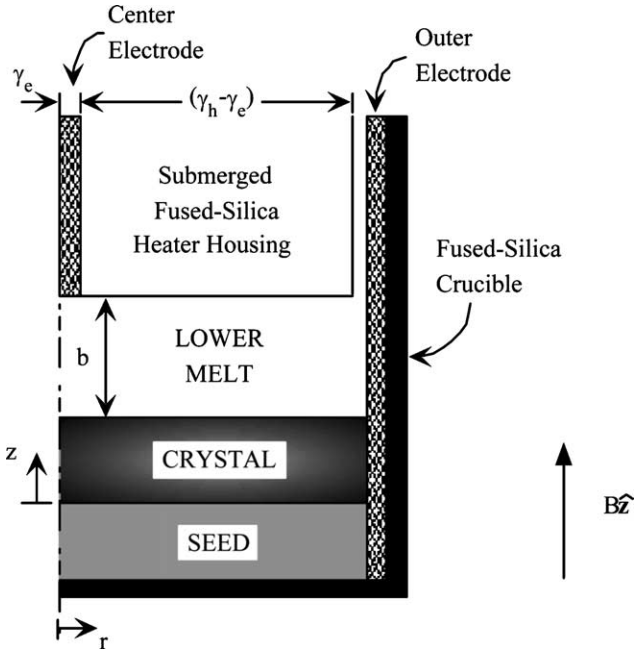

Fig. 1. VGF process using submerged heater growth with a uniform, steady, axial magnetic field $B\hat{\mathbf{z}}$ and with a steady radial electric current where coordinates are normalized by the outer electrode's inner radius.

that the depth of the melt is constant throughout growth. The heater is rotated at angular velocity ω, which is normalized by U_c/R. A long cylindrical graphite electrode at the centerline moves with the submerged heater and carries an axially downward constant DC electric current. The electrical conductivity of the graphite electrodes is much larger than that of either the molten semiconductor, the fused-silica heater housing or the crystal, so that the electric current travels through the long outer graphite electrode tube which rests inside the periphery of the crucible.

A magnetic field is applied with a copper coil outside the heater insulation, while an electric current is applied through the electrode so that the electromagnetic (EM) body force created by this electric current is balanced by the inertial force. This balance gives a characteristic velocity (Ma et al., 2003),

$$U_c = \left(\frac{BJ_cR}{\rho_0}\right)^{1/2}, \tag{1}$$

where R is the inner radius of the outer electrode or the radius of the crystal, and ρ_0 is the density of the molten semiconductor at the melting temperature T_m. Here, the characteristic electric current density is $J_c = I/(2\pi r_0 bR)$, where r_0 is a radial position that can be used to provide an approximate estimate of the radial electric current density. For a crystal grown with $R = 25$ mm, $b = 0.4$ and $r_0 = 1$ cm, and for electromagnetic stirring produced with $B = 0.004$ T and $I = 4$ A, our estimation of J_c is 6366.2 A/m^2 and the characteristic velocity is $U_c = 0.01027$ m/s.

The electric current in the melt produces an induced magnetic field which is superimposed upon the applied magnetic field produced by the external magnet. The characteristic ratio of the induced to applied magnetic field strengths is the magnetic Reynolds number, $R_m = \mu_p \sigma U_c R$, where μ_p is the magnetic permeability of the melt and σ is the electrical conductivity of the melt. For all crystal growth processes, $R_m \ll 1$ and the additional magnetic fields produced by the electric currents in the melt are negligible.

Ohm's law is

$$\mathbf{j} = -\nabla\phi + N\mathbf{v}\times\hat{\mathbf{z}}, \tag{2}$$

where $\mathbf{j}$ is the electric current density normalized by J_c, ϕ is the electric potential normalized by J_cR/σ, and $\mathbf{v} = v_r\hat{\mathbf{r}} + v_\theta\hat{\boldsymbol{\theta}} + v_z\hat{\mathbf{z}}$ is the melt velocity normalized by U_c. Here, the ratio of the induced electric field $\mathbf{v}\times\hat{\mathbf{z}}$ to the static electric field $\nabla\phi$ is the interaction parameter, $N = \sigma B^2 R/\rho_0 U_c$. For the present process with $B = 0.004$ T and $I = 4$ A, $N = 0.006$ so that the induced electric field is negligible. For our axisymmetric problem, there is no azimuthal flow of electric current, and the electric potential is governed by

$$\nabla^2\phi = 0. \tag{3}$$

We treat the electrodes as perfect conductors which carry a uniform electric potential. The boundary conditions are

$$\phi = 0, \quad \text{at } r = 1, \quad \text{for } -1 \leqslant \zeta \leqslant +1, \tag{4a}$$

$$\phi = \Phi_0, \quad \text{at } \zeta = +1, \quad \text{for } 0 \leqslant r \leqslant \gamma_e. \tag{4b}$$

Here, $\zeta = -1 + 2(z - \alpha t)/b$ is a rescaled axial coordinate so that $-1 \leqslant \zeta \leqslant +1$. The fused-silica heater, the annular gap between the heater and the outer electrode, and the crystal–melt interface are treated as electrical insulators so that $\hat{\mathbf{n}}\cdot\nabla\phi = 0$, where $\hat{\mathbf{n}}$ is the outward unit normal vector. The electric potential is given by a separation-of-variables solution,

$$\phi = \sum_{n=0}^{\infty} A_n \Phi_0 J_0(\lambda_n r)\frac{\cosh\left(\frac{\lambda_n b}{2}(\zeta+1)\right)}{\cosh(\lambda_n b)}, \tag{5}$$

where J_0 is the Bessel function of the first kind and zeroth order and λ_n are the eigenvalues of J_0. Based on our choice for the characteristic electric current density J_c, the integral of the radial electric current over the melt depth must equal b at $r = r_0$, so that

$$\Phi_0 = b\left[\sum_{n=1}^{\infty} A_n J_1 t(\lambda_n r_0)\frac{\sinh(\lambda_n b)}{\cosh(\lambda_n b)}\right]^{-1}, \tag{6}$$

where J_1 is the Bessel function of the first kind and first order. A Galerkin method is implemented to avoid a Gibb's phenomena associated with the discontinuous boundary conditions along $\zeta = +1$. The electric current originates from the center electrode and flows radially outward and axially downward, as reflected in the contours of the electric potential which are presented in Fig. 2 for $\gamma_e = 0.1905$ and $b = 0.4$ for which $\Phi_0 = 1.353$.

In a frame of reference moving with the fused-silica heater and crystal–melt interface, the melt motion is

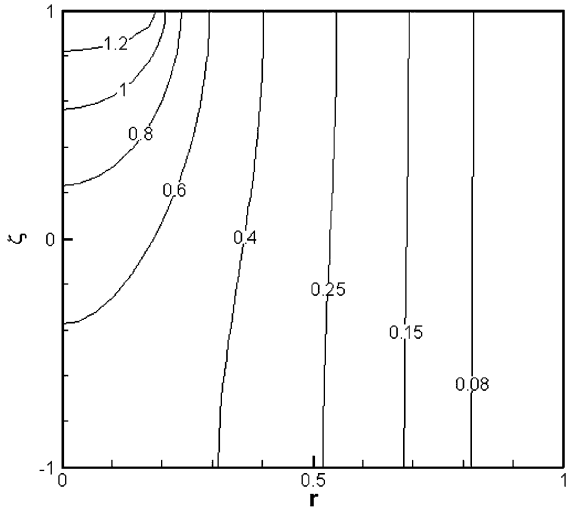

Fig. 2. Contours of the electric potential in the melt $\phi(r,\zeta)$ for $\gamma_e = 0.1905$ and $b = 0.4$.

steady. With the Boussinesq approximation, the equations governing the steady, axisymmetric melt velocity and temperature are

$$(\mathbf{v}\cdot\nabla)\mathbf{v} = -\nabla p + \Lambda T\hat{\mathbf{z}} + \frac{\partial\phi}{\partial r}\hat{\theta} + Re^{-1}\nabla^2\mathbf{v}, \tag{7a}$$

$$\nabla\cdot\mathbf{v} = 0, \tag{7b}$$

$$\mathrm{Pr}\, Re(\mathbf{v}\cdot\nabla)T = \nabla^2 T, \tag{7c}$$

where p is the deviation of the dimensional pressure from the hydrostatic pressure for a uniform density normalized by $\rho_0 U_c^2$, and T is the deviation of the dimensional temperature from the melting temperature T_m normalized by $(T_h - T_m)$. Here, the Prandtl number is $Pr = \mu c_p/k$ while the Reynolds number is $Re = \rho_0 U_c R/\mu$, where μ, c_p and k are the dynamic viscosity, specific heat and thermal conductivity of the melt, respectively. The Reynolds number is related to the strength of the electromagnetic stirring, i.e., Re is directly proportional to $(\mathrm{BI})^{1/2}$. In Eq. (7a), the ratio of the buoyancy force to the electromagnetic body force is $\Lambda = \rho_0 g\beta(T_h - T_m)/J_c B$, which we refer to as the electromagnetic (EM) buoyancy parameter. Here, $g = 9.81$ m^2/s and β is the thermal volumetric expansion coefficient.

We use a frame of reference moving with the heater and the crystal–melt interface, so the no-slip and no-penetration conditions on the surface of the outer electrode are

$$v_r = 0, \quad \text{at } r = 1, \quad \text{for } -1 \leqslant \zeta \leqslant +1, \tag{8a}$$

$$v_\theta = 0, \quad \text{at } r = 1, \quad \text{for } -1 \leqslant \zeta \leqslant +1, \tag{8b}$$

$$v_z = -\alpha, \quad \text{at } r = 1, \quad \text{for } -1 \leqslant \zeta \leqslant +1. \tag{8c}$$

The boundary conditions on the crystal–melt interface and on the surfaces of the center electrode, fused-silica heater and the annular gap between the heater and the crucible where the lower melt is replenished are

$$v_r = 0, \quad \text{at } \zeta = -1, \quad \text{for } 0 \leqslant r \leqslant 1, \tag{9a}$$

$$v_\theta = 0, \quad \text{at } \zeta = -1, \quad \text{for } 0 \leqslant r \leqslant 1, \tag{9b}$$

$$v_z = -\alpha, \quad \text{at } \zeta = -1, \quad \text{for } 0 \leqslant r \leqslant 1, \tag{9c}$$

$$v_r = 0, \quad \text{at } \zeta = +1, \quad \text{for } 0 \leqslant r \leqslant \gamma_h, \tag{9d}$$

$$v_\theta = \omega r, \quad \text{at } \zeta = +1, \quad \text{for } 0 \leqslant r \leqslant \gamma_h, \tag{9e}$$

$$v_\theta = \frac{\omega\gamma_h^2}{1-\gamma_h^2}\left(\frac{1}{r} - r\right), \quad \text{at } \zeta = +1, \quad \text{for } \gamma_h \leqslant r \leqslant 1, \tag{9f}$$

$$v_z = 0, \quad \text{at } \zeta = +1, \quad \text{for } 0 \leqslant r \leqslant \gamma_h, \tag{9g}$$

$$v_z = f(r), \quad \text{at } \zeta = +1, \quad \text{for } \gamma_h \leqslant r \leqslant 1. \tag{9h}$$

We use simple analytical solutions to approximate the azimuthal and axial flows of the replenished fluid in the gap. In. Eq. (9f), we approximate the azimuthal velocity with a Taylor-Couette flow which satisfies the no-slip conditions given by Eqs. (8b) and (9e). In Eq. (9h), the axial velocity of the fluid that is replenished through the gap is approximated with a Couette flow. Assuming that the density of the crystal and melt are the same, the gap between the heater and the outer electrode replenishes the solidifying melt at a volumetric flowrate $\pi\alpha$, so that $f(r)$ given by

$$f(r) = \alpha[-1 + \kappa_1(1-r) + \kappa_2(1-r^2)], \tag{10a}$$

where

$$\kappa_1 = \frac{3(1+\gamma_h^2)}{(1-\gamma_h)^3}, \quad \kappa_2 = -\frac{2(1+\gamma_h+\gamma_h^2)}{(1-\gamma_h)^3(1+\gamma_h)}, \tag{10b, 10c}$$

which satisfies the no-slip conditions given by Eqs. (8c) and (9g).

The thermal boundary conditions are

$$T = 0, \quad \text{at } \zeta = -1, \quad \text{for } 0 \leqslant r \leqslant 1, \tag{11a}$$

$$T = 1, \quad \text{at } \zeta = +1, \quad \text{for } 0 \leqslant r \leqslant 1, \tag{11b}$$

$$\frac{\partial T}{\partial r} = 0, \quad \text{at } r = 1, \quad \text{for } -1 \leqslant \zeta \leqslant +1. \tag{11c}$$

We have assumed that the rate of heat transfer from the outer electrode to the melt is negligible.

We introduce a Stokes stream function for the radial and axial velocities in the meridional circulations,

$$v_r = \frac{1}{r}\frac{\partial\psi}{\partial z}, \quad v_z = -\frac{1}{r}\frac{\partial\psi}{\partial r}, \tag{12a, 12b}$$

which identically satisfies conservation of mass for our axisymmetric melt motion. For given values of Λ, Pr and Re, we solved for ψ, v_θ and T using a Chebyshev spectral collocation method with Gauss-Lobatto collocation points in r and ζ. Since Eqs. (7a) and (7c) are non-linear, we used a Newton–Raphson iterative method, and incrementally increased Re from zero. After the Newton–Raphson method converged for a given Re, we used a continuation method to obtain initial guesses for the coefficients in the spectral representations for $(Re + \Delta Re)$. For each value of Re, the numbers of collocation points was varied in order to insure that the results were independent of this numbers and to insure that all boundary layers were adequately resolved. For example, for $Re = 60$ and $\omega = 0.8542$, we used 46 collocation points in the radial direction and 41 collocation points in the axial direction. When we doubled the collocation points in the radial direction, the minimum value of the azimuthal velocity changed by 0.03% and the maximum value of azimuthal velocity changed by 0.03%. When we doubled the collocation points in the axial direction, the minimum and maximum values of the azimuthal velocity changed by only 0.0001%.

3. Results

We investigate the effects of electromagnetic stirring and heater rotation on the melt motion with $\gamma_h = 0.8$, $Pr = 0.0442$, $b = 0.4$, and $U_g = 2$ mm/h for a gallium-antimonide melt. The parameters as a function of the characteristic velocity are $Re = 65{,}259.7U_c$, $Pe_t = 2891.58U_c$, $\Lambda = 0.0004697U_c^{-2}$, and $\alpha = 5.556 \times 10^{-7} U_c^{-1}$, where U_c is in m/s. The thermophysical properties of gallium-antimonide are presented in Table 1. The characteristic velocities and dimensionless parameters are summarized in Table 2.

For $Re = 60$, the characteristic velocity is $U_c = 0.0009194$ m/s. The dimensionless parameters are $Pe_t = 2.659$, $\Lambda = 555.7$, and $\alpha = 0.0006043$. We present results for a static heater with $\omega = 0$. In Fig. 3a–c, we present contours of the azimuthal velocity $v_\theta(r, \zeta)$, the meridional streamfunction $\psi(r, \zeta)$, and the temperature $T(r, \zeta)$, respectively. In Fig. 3a, the electromagnetic (EM) body force drives a clockwise azimuthal melt motion and the minimum and maximum values of v_θ are -0.9248 and 0, respectively. This minimum value corresponds to a dimensional azimuthal velocity of -0.0008503 m/s. In Fig. 3b, there are two opposing circulations in the meridional melt motion and the minimum and maximum values of $\psi(r, \zeta)$ are -0.002401 and 0.001675, respectively. In Fig. 3c, we can see that

Table 1
Thermophysical properties for molten GaSb

Property	Value
Density, ρ_0 (kg/m^3)	6030
Dynamic viscosity, μ (Pa s)	0.00231
Thermal conductivity, k (W/m K)	17.1
Specific heat, c_p (J/kg · K)	328
Electrical conductivity, σ (S/m)	1×10^6
Thermal coefficient of volumetric expansion, β_T (K^{-1})	0.0000958

Table 2
Characteristic velocities and dimensionless parameters

	$U_c = 0.0009194$ m/s	$U_c = 0.0004597$ m/s
Re	60	30
Pe_t	2.659	1.3293
Λ	555.7	2222
α	0.0006043	0.001209

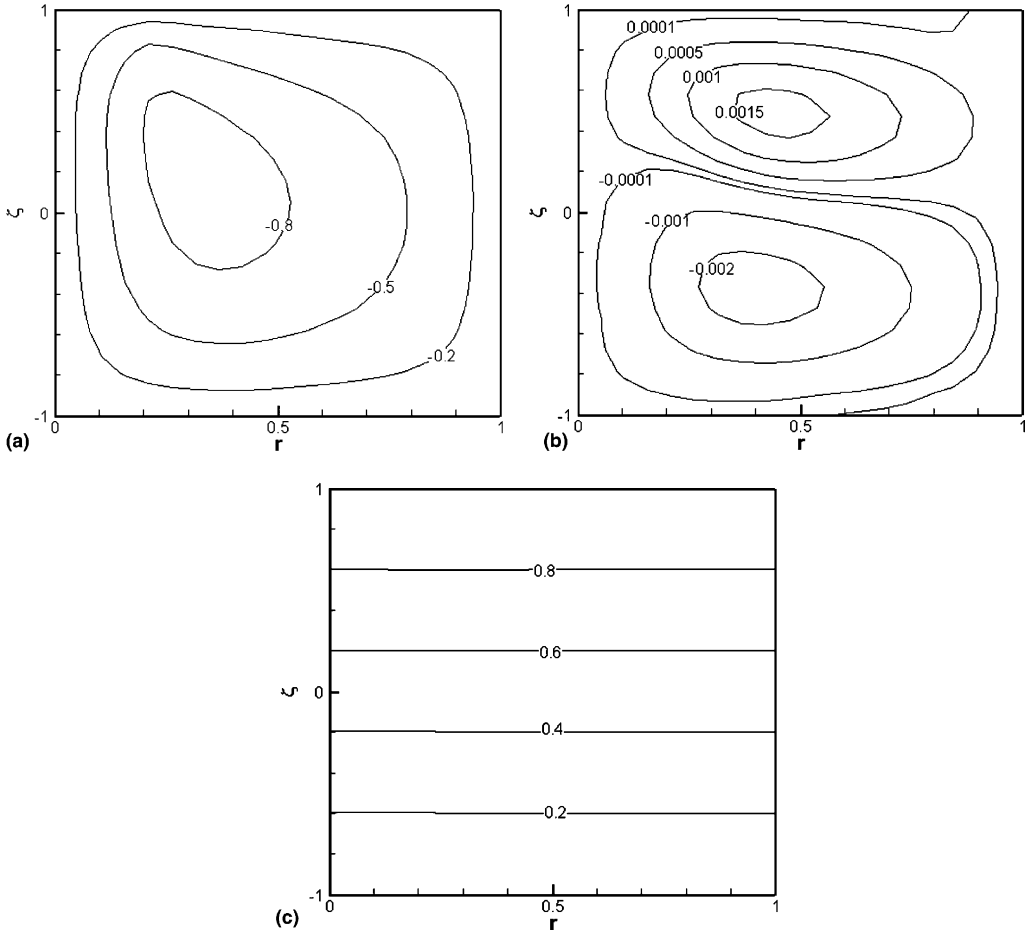

Fig. 3. Contours for the steady-state melt motion with $Re = 60$ and $\omega = 0$: (a) azimuthal velocity $v_\theta(r, \zeta)$, (b) meridional streamfunction $\psi(r, \zeta)$, (c) temperature $T(r, \zeta)$.

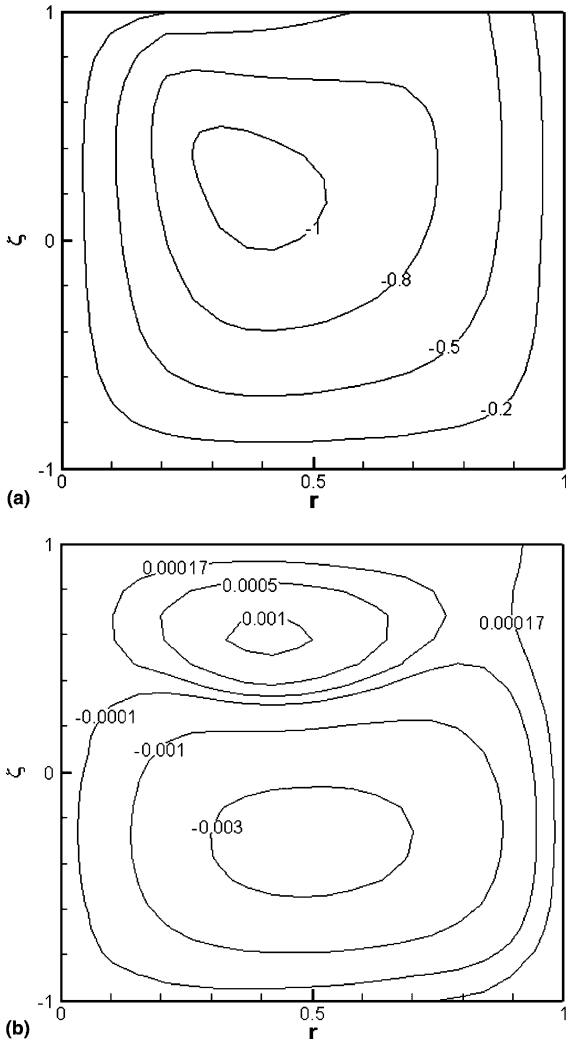

Fig. 4. Contours for the steady-state melt motion with $Re = 60$ and $\omega = -0.8542$: (a) azimuthal velocity $v_\theta(r, \zeta)$, (b) meridional streamfunction $\psi(r, \zeta)$.

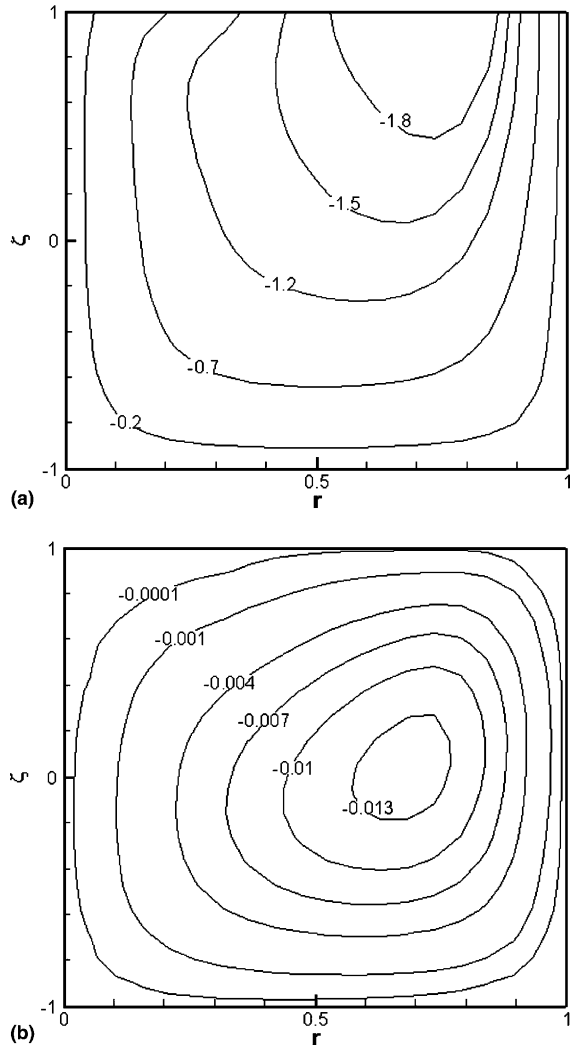

Fig. 5. Contours for the steady-state melt motion with $Re = 60$ and $\omega = -3.1417$: (a) azimuthal velocity $v_\theta(r, \zeta)$, (b) meridional streamfunction $\psi(r, \zeta)$.

the heat transfer is dominated by conduction. The temperature gradient is primarily axial with a slight radial gradient.

A clockwise rotation of the heater for $\omega < 0$ augments the EM stirring. For $Re = 60$ and $\omega = -0.8542$ which corresponds to a rotation rate of -0.3 rpm, we present contours of the azimuthal velocity and the meridional streamfunction in Fig. 4a and b, respectively. The isotherms are very similar to those for $\omega = 0$ in Fig. 3c in which the heat transfer is dominated by conduction. In Fig. 4a, the heater's rotation has decreased the minimum value of v_θ to -1.0502 and the contours are no longer closed. This minimum value corresponds to a dimensional azimuthal velocity of -0.0009656 m/s. In Fig. 4b, the lower circulation takes a much larger volume of the melt compared with the $\omega = 0$ case. The magnitude of the radially inward flow along the crystal–melt interface has increased. The minimum and maximum values of ψ are -0.003838 and 0.001125, respectively.

We rotate the heater more quickly at $\omega = -3.1417$ which corresponds to a rotation rate of -1.2 rpm. Contours of the azimuthal velocity and the meridional streamfunction are presented in Fig. 5a and b, respectively. The isotherms are very similar to those for $\omega = 0$ in Fig. 3c in which the heat transfer is dominated by conduction. With this faster rotation rate, the minimum value of v_θ has further decreased to -2.694. This minimum value corresponds to a dimensional azimuthal velocity of -0.002477 m/s. The increased centrifugal body force is reflected in Fig. 5a where the contours of the azimuthal velocity are nearly dominated by the flow due to rotation. When we further increased the rotation rate, the rotational flow dominated the EM stirring. In Fig. 5b, the minimum and maximum values of the meridional streamfunction ψ are -0.01418 and 0.0003021, respectively. The lower circulation has grown and takes the entire volume of the melt, in which the melt flows radially inward along the crystal–melt

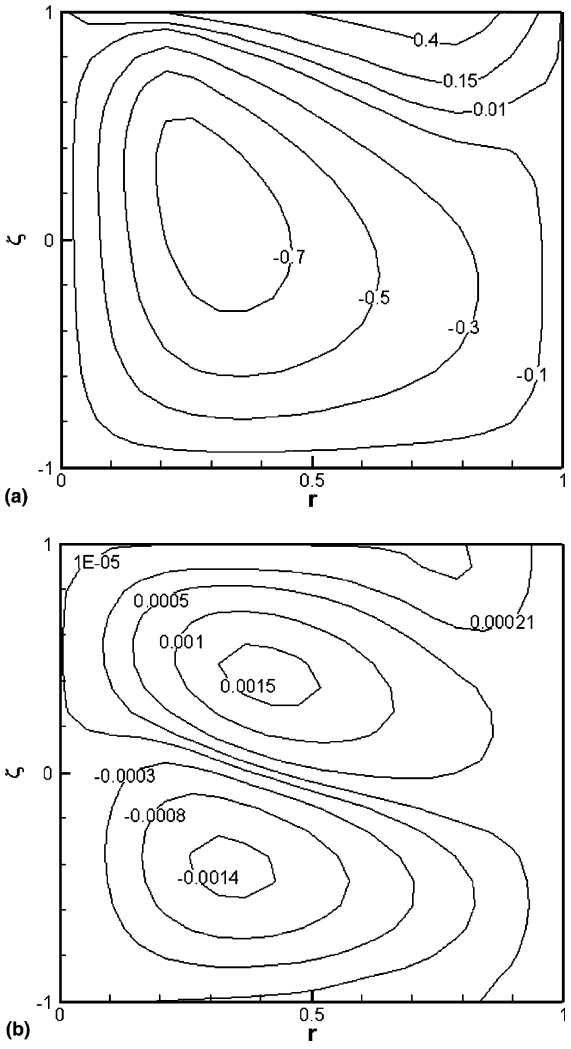

Fig. 6. Contours for the steady-state melt motion with $Re = 60$ and $\omega = 0.8542$: (a) azimuthal velocity $v_\theta(r, \zeta)$, (b) meridional streamfunction $\psi(r, \zeta)$.

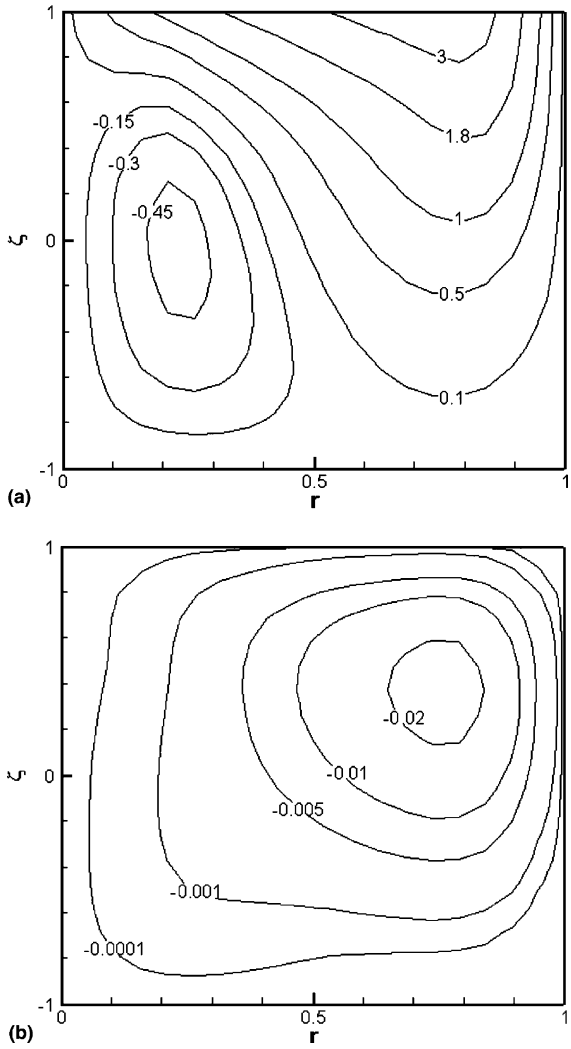

Fig. 7. Contours for the steady-state melt motion with $Re = 60$ and $\omega = 5.6950$: (a) azimuthal velocity $v_\theta(r, \zeta)$, (b) meridional streamfunction $\psi(r, \zeta)$.

interface, axially upward along the centerline, radially outward along the heater and axially downward along the periphery of the melt.

For $Re = 60$, we investigate a counterclockwise rotation of the heater for which $\omega > 0$. Because the EM stirring drives a clockwise azimuthal melt motion, a counterclockwise rotation of the heater opposes the EM stirring. For $\omega = 0.8542$, Fig. 6a and b show the contours of the azimuthal velocity and the meridional streamfunction, respectively. The isotherms are very similar to those for $\omega = 0$ in Fig. 3c where the heat transfer remains dominated by conduction. In Fig. 6a, the minimum and maximum values of v_θ are -0.8120 and 0.6735, respectively. These minimum and maximum values correspond to dimensional values of -0.0007465 m/s and 0.0006192 m/s, respectively. In Fig. 6b, the minimum and maximum values of ψ are -0.001553 and 0.001659, respectively. The magnitude of the radially inward flow along the crystal–melt interface has decreased compared with $\omega = 0$.

For $Re = 60$, we rotate the heater more quickly at angular velocity $\omega = 5.6950$ which corresponds to a rotation rate of 2.0 rpm. Contours of the azimuthal velocity and the meridional streamfunction are presented in Fig. 7a and b, respectively. The isotherms are very similar to those for $\omega = 0$ in Fig. 3c in which the heat transfer is dominated by conduction. With the quicker rotation of the submerged heater, the minimum and maximum values of v_θ have further increased to -0.4992 and 4.4903, respectively. These minimum and maximum values correspond to dimensional values of -0.0004590 m/s and 0.004128 m/s, respectively. In Fig. 7b, the lower circulation takes the whole volume of the melt. The minimum and maximum values of ψ are -0.02381 and 0.0003021, respectively. The minimum and maximum values of the azimuthal velocity and

Table 3
Minimum and maximum values of v_θ and ψ

Re	ω^* (rpm)	ω	$v_{\theta,\min}$	$v_{\theta,\max}$	$\psi_{\min}$	$\psi_{\max}$
60	−1.2	−3.1417	−2.694	0	−0.01418	0.0003021
60	−0.3	−0.8542	−1.0502	0	−0.003838	0.001125
60	0	0	−0.9248	0	−0.002401	0.001675
60	0.3	0.8542	−0.8120	0.6735	−0.001553	0.001659
60	2.0	5.6950	−0.4992	4.4903	−0.02381	0.0003021
30	−0.3	−1.7085	−1.3471	0	−0.001987	0.0006043
30	0.3	1.7085	−0.2840	1.3471	−0.0009759	0.0006043

meridional streamfunction are summarized in Table 3, where ω^* is the dimensional rotation rate in rpm.

For $Re = 30$, the characteristic velocity is $U_c = 0.0004597$ m/s, and the dimensionless parameters are $Pe_t = 1.3293$, $\Lambda = 2222$, and $\alpha = 0.001209$. For a clockwise rotation $\omega = -1.7085$ for which the rotation rate is −0.3 rpm, we present the contours of the azimuthal velocity and meridional streamfunction in Fig. 8a and b respectively. The isotherms are very similar to those for $\omega = 0$ in Fig. 3c in which the heat transfer is dominated by conduction. In Fig. 8a, the minimum and maximum values of v_θ are −1.3471 and 0, respectively. This minimum value corresponds to a dimensional azimuthal velocity of −0.0006193 m/s. The clockwise rotational flow reinforces the clockwise EM stirring. Compared with $Re = 60$ and a rotation rate of −0.3 rpm,

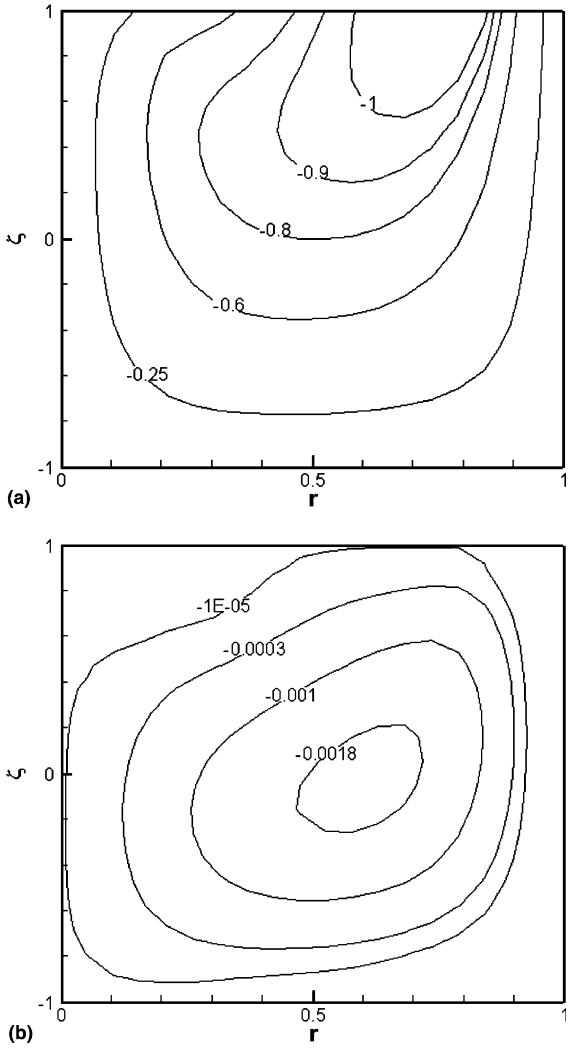

Fig. 8. Contours for the steady-state melt motion with $Re = 30$ and $\omega = -1.7085$: (a) azimuthal velocity $v_\theta(r, \zeta)$, (b) meridional streamfunction $\psi(r, \zeta)$.

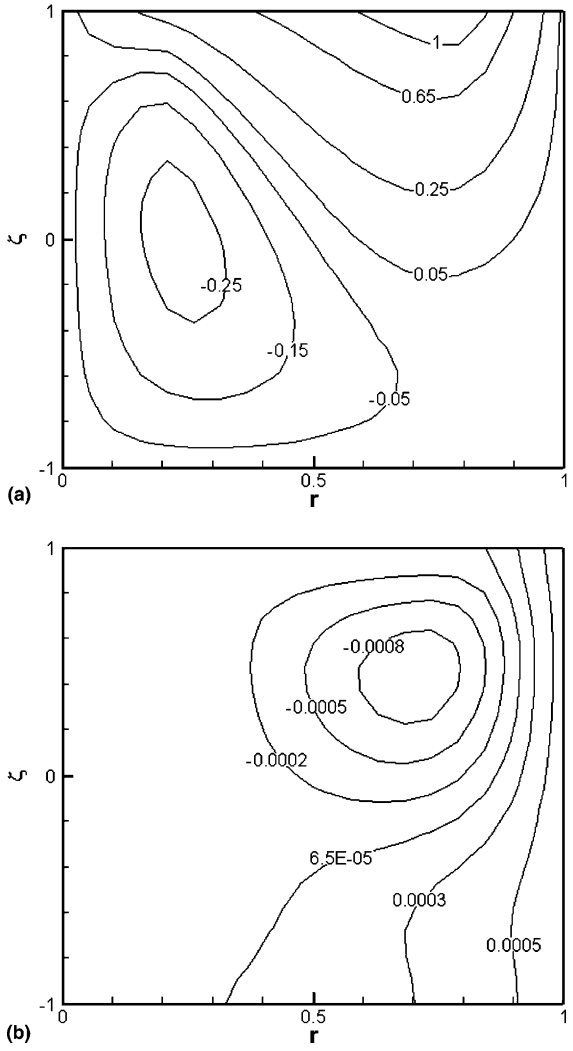

Fig. 9. Contours for the steady-state melt motion with $Re = 30$ and $\omega = 1.7085$: (a) azimuthal velocity $v_\theta(r, \zeta)$, (b) meridional streamfunction $\psi(r, \zeta)$.

the contours of v_θ in Fig. 8a reflect a much stronger rotational flow due to the decreased EM stirring for $Re = 30$. Because the magnitude of the EM stirring is proportional to $(BI)^{1/2}$, the relative importance of EM stirring to the rotational flow has decreased significantly. In Fig. 8b, the minimum and maximum values of ψ are -0.001987 and 0.0006043, respectively.

For $Re = 30$ with a counterclockwise rotation $\omega = 1.7085$ which corresponds to a rotation rate of 0.3 rpm, the contours of the azimuthal velocity and meridional streamfunction are presented in Fig. 9a and b, respectively. The isotherms are very similar to those for $\omega = 0$ in Fig. 3c in which the heat transfer is dominated by conduction. In Fig. 9a, the minimum and maximum values of v_θ are -0.2840 and 1.3471, respectively. These minimum and maximum values correspond to dimensional values of -0.0001306 m/s and 0.0006192 m/s, respectively. In Fig. 9b, the minimum and maximum values of ψ are -0.0009759 and 0.0006043, respectively. Compared with $Re = 60$ and a rotation rate of 0.3 rpm, the rotational flow more strongly opposes the EM stirring. The minimum and maximum values of the azimuthal velocity and meridional streamfunction are summarized in Table 3.

4. Conclusions

For vertical gradient freezing growth using a submerged heater with weak magnetic and electric fields, the application of heater rotation can have a strong influence on the melt motion. A larger radially inward flow adjacent to the crystal–melt interface is desirable because it would promote compositional uniformity in the crystal. A clockwise heater rotation augments the electromagnetic (EM) stirring while a counterclockwise heater rotation opposes the EM stirring. The magnitude of the radially inward flow adjacent to the crystal–melt interface increases as the Reynolds number (or EM stirring) increases and as the rotation of the heater in the clockwise direction increases.

Acknowledgements

This research was supported by the US Air Force Office of Scientific Research under grant FA9550-04-1-0249 and by the NRC/USAF Office of Scientific Research Summer Faculty Fellowship Program. The calculations were performed on the Cray X1 and the SGI Origin 3000 Complex provided by the DoD High Performance Computing Modernization Program under grant AFSNH2487 and on the IBM pSeries 690 provided by the National Computational Science Alliance.

References

Farrell, M.V., Ma, N., 2004. Macrosegregation during alloyed semiconductor crystal growth in strong axial and transverse magnetic fields. International Journal of Heat and Mass Transfer 47, 3047–3055.

Kuniholm, J.F., Ma, N., 2003. Natural convection in a liquid-encapsulated molten semiconductor with a steady magnetic field. International Journal of Heat and Fluid Flow 24, 130–136.

Ma, N., Bliss, D.F., Iseler, G.W., 2003. Vertical gradient freezing of doped gallium-antimonide semiconductor crystals using submerged heater growth and electromagnetic stirring. Journal of Crystal Growth 259, 26–35.

Meyer, S., Ostrogorsky, A.G., 1997. Forced convection in vertical Bridgman configuration with the submerged heater. Journal of Crystal Growth 171, 566–576.

Morton, J.L., Ma, N., Bliss, D.F., Bryant, G.G., 2002. Dopant segregation during liquid-encapsulated Czochralski crystal growth in a steady axial magnetic field. Journal of Crystal Growth 242, 471–485.

Ohmori, Y., Sugii, K., Akai, S., Matsumoto, K., 1982. LEC growth of Te-doped GaSb single crystals with uniform carrier concentration distribution. Journal of Crystal Growth 60, 79–85.

Ostrogorsky, A.G., 1990. Numerical simulation of single crystal growth by submerged heater method. Journal of Crystal Growth 104, 233–238.

Ostrogorsky, A.G., Müller, G., 1994. Normal and zone solidification using the submerged heater method. Journal of Crystal Growth 137, 64–71.

Wang, X., Ma, N., Bliss, D.F., Iseler, G.W., 2005. Semiconductor crystal growth by modified vertical gradient freezing with electromagnetic stirring. Journal of Thermophysics and Heat Transfer 19, 95–100.